# Polarized electrolyte-electroreflectance study of $ReS_2$ and $ReSe_2$ layered semiconductors



2001 J. Phys.: Condens. Matter 13 8145

(http://iopscience.iop.org/0953-8984/13/35/319)

INSTITUTE OF PHYSICS PUBLISHING JOURNAL OF PHYSICS: CONDENSED MATTER

J. Phys.: Condens. Matter **13** (2001) 8145–8152 PII: S0953-8984(01)25452-6

# Polarized electrolyte-electroreflectance study of $ReS_2$ and $ReSe_2$ layered semiconductors

**C H Ho[1,4], P C Yen[2], Y S Huang[2] and K K Tiong[3]**

[1] Department of Electronic Engineering, Kuang Wu Institute of Technology, Peitou, Taipei 112, Taiwan, Republic of China
[2] Department of Electronic Engineering, National Taiwan University of Science and Technology, Taipei 106, Taiwan, Republic of China
[3] Department of Electrical Engineering, National Taiwan Ocean University, Keelung 202, Taiwan, Republic of China

E-mail: chhwho@ms28.hinet.net

Received 4 June 2001
Published 16 August 2001
Online at stacks.iop.org/JPhysCM/13/8145

**Abstract**

Polarization dependent electrolyte-electroreflectance (EER) measurements of $ReS_2$ and $ReSe_2$ layered crystals have been carried out in the energy range of 1.3 to 5.0 eV. The EER spectra of $\boldsymbol{E} \parallel \boldsymbol{b}$ polarization exhibit distinct band-edge excitonic and interband transition features from those of $\boldsymbol{E} \perp \boldsymbol{b}$ polarization. Analysing the polarization dependent EER spectra, the structures of the excitonic and interband transitions of $ReS_2$ and $ReSe_2$ with optical polarizations along the $\boldsymbol{b}$-axis and perpendicular to the $\boldsymbol{b}$-axis are examined clearly and the energy positions are determined accurately. The mechanism of field–lattice interaction is proposed to account for the in-plane anisotropy of the crystals. Based on the analysis of experimental results, a probable band-structure scheme of $ReX_2$ (X = S, Se) is constructed.

## 1. Introduction

Layered crystals of $ReX_2$ (X = S, Se) are diamagnetic semiconductors that belong to the family of the transition-metal dichalcogenides (TMDCs) crystallizing in the distorted octahedral layer structure of triclinic symmetry [1,2]. $ReX_2$ (X = S, Se) are indirect semiconductors and the energy gaps are 1.37 eV for $ReS_2$ and 1.19 eV for $ReSe_2$, respectively [3, 4]. Layered $ReX_2$ are of considerable interest for various applications due to their optical, electrical and mechanical properties [1]. These applications include a sulphur-tolerant hydrogenation and hydrodesulphurization catalyst [5, 6] and as a promising solar-cell material in electrochemical cells [7, 8]. Unlike most of the layered TMDCs, $ReX_2$ crystallizes in a distorted $CdCl_2$-type layer structure with triclinic symmetry. A clustering pattern of 'diamond chains'

[4] Author to whom correspondence should be addressed.

  

consisting of Re ions forms along the $\boldsymbol{b}$-axis in the $ReX_2$ monolayer resulting in the crystals being optically biaxial. Therefore, an anisotropic response of $ReX_2$ is expected for linearly polarized light incident normal to the basal plane. The in-plane anisotropic properties of $ReX_2$ may be exploited for fabrication of polarization sensitive photodetectors [9]. Despite the various technological applications, very few experimental studies [4, 9, 19] on the anisotropic characteristics of the electronic structure of $ReX_2$ have been reported due most probably to the inherent difficulty of performing the polarization dependence experiment over a wide energy range.

In this paper we present for the first time the polarization-dependent electrolyte electroreflectance (EER) spectra of $ReS_2$ and $ReS_2$ in the energy range of 1.3 to 5 eV. The EER measurements are carried out with linearly polarized light ($\boldsymbol{E} \parallel \boldsymbol{b}$ and $\boldsymbol{E} \perp \boldsymbol{b}$ polarizations) incident normal to the van der Waals plane. As shown in figure 1, the $\boldsymbol{b}$- and $\boldsymbol{a}$-axes are the shortest and second shortest axes in the basal plane of $ReX_2$. The $\boldsymbol{b}$-axis is parallel to the Re cluster chains, which corresponds to the longest edge of the plate [9, 10]. The EER technique has been proven to be a very powerful tool in the study of the electronic band structure of semiconductors [11, 12]. The polarized EER measurements enable us to discriminate different in-plane anisotropic transitions from various linearly polarized light. The EER spectra are fitted with a form of the Aspnes equation of the derivative Lorentzian lineshape [13]. From detailed lineshape fits, the transition energies of the band-edge excitonic and higher lying interband transitions are determined accurately. The mechanism of field-lattice interaction is being proposed to account for the in-plane anisotropy of the crystals. Combining the results with previous theoretical [15, 17] and experimental works [4, 16–19] on the $ReS_2$ and $ReSe_2$ materials, a probable band-structure scheme of $ReX_2$ (X = S, Se) is then constructed.

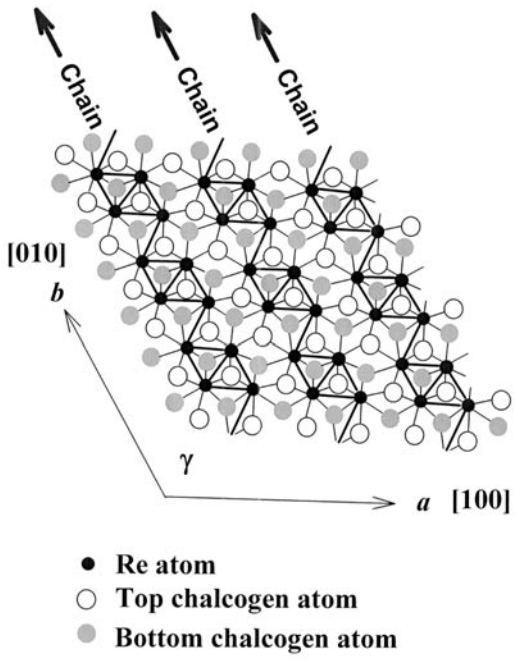


**Figure 1.** Representative scheme of the van der Waals plane of $ReX_2$ (X = S, Se) layered crystals. The '$Re_4$' clustering chains that correspond to the crystal orientation of the $\boldsymbol{b}$-axis are illustrated.

## 2. Experimental details

Single crystals of $ReS_2$ and $ReSe_2$ were grown using the chemical vapour transport method with $Br_2$ as the transport agent. Prior to the crystal growth, quartz tubes containing bromine and the elements (Re, 99.95% pure; S, 99.999%; Se, 99.999%) were evacuated and sealed. To improve the stoichiometry, sulphur or selenium with 2 mol% in excess was added with respect to rhenium. The quartz tube was placed in a three-zone furnace and the charge prereacted for 24 h at 800 °C while the temperature of the growth zone was set at 1000 °C to prevent the transport of the product. The furnace was then equilibrated to give a constant temperature across the reaction tube, and was programmed over 24 h to produce the temperature gradient at which single crystal growth takes place. Best results were obtained with temperature gradients of about 1060 → 1010 °C for $ReS_2$ and 1050 → 1000 °C for $ReSe_2$. Both $ReS_2$ and $ReSe_2$ formed thin, silver-coloured, graphite-like, hexagonal platelets up to 2 $cm^2$ in area and 100 $\mu$m in thickness. X-ray diffraction patterns of single crystals confirmed the triclinic symmetry of $ReS_2$ and $ReSe_2$ with all parameters consistent with those previously reported [2, 20, 21]. Electron probe microanalysis indicated a slight chalcogen deficiency in the crystals. Hall measurements revealed n-type semiconducting behaviour. The electrical resistivities of $ReS_2$ and $ReSe_2$ at 300 K are 120 and 26 Ω cm, respectively.

The EER spectra were taken on a fully computerized setup for modulation spectroscopy described elsewhere [20]. The detector response to the DC component of the reflected light is kept constant by either an electronic servo mechanism or a neutral density filter so that the AC reflectance corresponds to $\Delta R/R$, the differential reflectance. Scans of $\Delta R/R$ versus wavelength are obtained using a 0.35 m grating monochromator together with a 150 W xenon arc lamp as a monochromatic light source. A pair of Glan–Taylor-prism polarizers with the measured range of 215–1000 nm is employed for polarization dependent measurements. Plate-shaped crystals were selected for the measurements. The electrolyte was a 1 N $H_2SO_4$ aqueous solution, and the counter-electrode was a 5 $cm^2$ platinum (Pt) plate. A 200 Hz, 100 mV peak to peak, square wave with zero DC bias applying between $ReX_2$ and the counter Pt electrodes was used to modulate the electric field in the space charge region. The modulated field between the $ReX_2$ and Pt electrodes must be confirmed within the low-field limits by using current-voltage (I-V) measurement so as the EER line shape is DC bias independent and the amplitude of signal varied linearly proportional to the AC modulation voltage.

## 3. Results and discussion

The polarization-dependent EER measurements were performed on four samples of $ReX_2$ from different growth batches. Similar spectral responses for either $\boldsymbol{E} \parallel \boldsymbol{b}$ or $\boldsymbol{E} \perp \boldsymbol{b}$ polarizations were obtained for different samples. The EER spectra of $ReS_2$ and $ReSe_2$ from one of the growth batches with optical polarizations along the $\boldsymbol{b}$-axis and perpendicular to the $\boldsymbol{b}$-axis, and the unpolarized spectra in the energy range of 1.3–5 eV are illustrated in figures 2(a) and 2(b). A multitude of interband transition features are observed in the EER spectra due to the nature of the triclinic low-symmetry structures of $ReX_2$. The $\boldsymbol{E} \parallel \boldsymbol{b}$ polarized spectra for both crystals exhibit distinct transition features from those of the $\boldsymbol{E} \perp \boldsymbol{b}$ polarization. The unpolarized EER spectra can be regarded as a result of random superposition of the two polarized spectra. In both figures 2(a) and 2(b), the $\boldsymbol{E} \parallel \boldsymbol{b}$ and $\boldsymbol{E} \perp \boldsymbol{b}$ polarization spectra showed two features, $E_1^{ex}$ and $E_2^{ex}$, more prominent than the rest. These features are related to the previously identified band-edge excitonic transitions [16, 18, 19]. By fitting the polarized EER spectra with the Aspnes derivative line shape expressions [13], we can determine the position of the interband transitions to accuracy better than 5 meV. Listed in tables 1 and 2 are, respectively, the

**Table 1.** Energy positions of the excitonic and interband transitions observed in the polarized EER spectra of $ReS_2$ together with the assignments of transition origins. The subscripts '$\parallel$' and '$\perp$' respectively refer to the $\boldsymbol{E} \parallel \boldsymbol{b}$ and $\boldsymbol{E} \perp \boldsymbol{b}$ polarizations.

| Feature | Energy position (eV) | The assignments of transition origins |
|---|---|---|
| $E_1^{ex}$ [a] | $1.485 \pm 0.005$ | Nonbonding Re 5d $t_{2g} \rightarrow$ nonbonding Re 5d $t_{2g}^*$ |
| $E_2^{ex}$ [a] | $1.519 \pm 0.005$ | Nonbonding Re 5d $t_{2g} \rightarrow$ nonbonding Re 5d $t_{2g}^*$ |
| $A$ [a] | $1.569 \pm 0.005$ | Nonbonding Re 5d $t_{2g} \rightarrow$ S 3p states |
| $A'$ [a] | $1.576 \pm 0.005$ | Nonbonding Re 5d $t_{2g} \rightarrow$ S 3p states |
| $E_1^{ex}$ [b] | $1.485 \pm 0.005$ | Nonbonding Re 5d $t_{2g} \rightarrow$ nonbonding Re 5d $t_{2g}^*$ |
| $E_2^{ex}$ [b] | $1.521 \pm 0.005$ | Nonbonding Re 5d $t_{2g} \rightarrow$ nonbonding Re 5d $t_{2g}^*$ |
| $C_\parallel$ [b] | $1.612 \pm 0.005$ | Nonbonding Re 5d $t_{2g} \rightarrow$ sulfur 3p states |
| $C_\perp$ [b] | $1.625 \pm 0.005$ | Nonbonding Re 5d $t_{2g} \rightarrow$ sulfur 3p states |
| $D_\parallel$ [b] | $2.00 \pm 0.01$ | Re 5d/S 3p bonding $\rightarrow$ Re 5d/S 3p antibonding |
| $D_\perp$ [b] | not observed | |
| $E_\parallel$ or $E_\perp$ [b] | $2.26 \pm 0.01$ | Re 5d/S 3p bonding $\rightarrow$ Re 5d/S 3p antibonding |
| $F_\parallel$ [b] | $2.49 \pm 0.01$ | Re 5d/S 3p bonding $\rightarrow$ Re 5d/S 3p antibonding |
| $F_\perp$ [b] | not observed | |
| $G_\parallel$ or $G_\perp$ [b] | $2.87 \pm 0.01$ | Re 5d/S 3p bonding $\rightarrow$ Re 5d/S 3p antibonding |
| $H_\parallel$ or $H_\perp$ [b] | $3.01 \pm 0.01$ | Re 5d/S 3p bonding $\rightarrow$ Re 5d/S 3p antibonding |
| $I_\parallel$ [b] | $3.33 \pm 0.01$ | Re 5d/S 3p bonding $\rightarrow$ Re 5d/S 3p antibonding |
| $I_\perp$ [b] | not observed | |
| $J_\parallel$ or $J_\perp$ [b] | $3.72 \pm 0.01$ | Re 5d/S 3p bonding $\rightarrow$ Re 5d/S 3p antibonding |
| $K_\parallel$ [b] | not observed | |
| $K_\perp$ [b] | $4.08 \pm 0.01$ | Re 5d/S 3p bonding $\rightarrow$ Re 5d/S 3p antibonding |
| $L_\parallel$ [b] | not observed | |
| $L_\perp$ [b] | $4.34 \pm 0.01$ | Re 5d/S 3p bonding $\rightarrow$ Re 5d/S 3p antibonding |
| $M_\parallel$ [b] | not observed | |
| $M_\perp$ [b] | $4.67 \pm 0.01$ | Re 5d/S 3p bonding $\rightarrow$ Re 5d/S 3p antibonding |

[a] Room temperature PzR results of [19].
[b] This work.

energy positions of the interband transitions of $ReS_2$ and $ReSe_2$ obtained from the polarization-dependent EER spectra together with the assignments of their physical origins. The energies values of the first two features from the room temperature polarized piezoreflectance (PzR) spectra of $ReS_2$ and $ReSe_2$ are also included for comparison [19, 25]. In [19], the features A for $\boldsymbol{E} \parallel \boldsymbol{b}$ and $A'$ for $\boldsymbol{E} \perp \boldsymbol{b}$ correspond to $C_\parallel$ and $C_\perp$ respectively for this work on $ReS_2$. A good match is observed for both sets of data. It is also noted that the present polarized EER data on $ReS_2$ represent a significant improvement over our previously published unpolarized EER measurements [18] on a similar $ReS_2$ sample. Comparing the results with those of the previous DOS calculations [17] of $ReS_2$ and $ReSe_2$, it is possible to associate the features with appropriate interband transitions. At present, although the structures originating from $\boldsymbol{E} \parallel \boldsymbol{b}$ and $\boldsymbol{E} \perp \boldsymbol{b}$ polarizations have been classified from the polarized EER experiments, the precise location of each critical-point transition may not be determined exactly. Nevertheless, this work will prove to be useful in aiding such identification when a more detailed theoretical band structure calculation including the effect of the in-plane anisotropy is available. The differences in the observed features for $\boldsymbol{E} \parallel \boldsymbol{b}$ and $\boldsymbol{E} \perp \boldsymbol{b}$ polarizations also lend evidence to the manifestation of another mechanism as pointed out by Weiser [23], namely the effect of field-induced polarization of the lattice. The mechanism leads to a displacement of the lattice atoms, which may alter the electronic states of the solids. The lattice-field interaction expected to be more pronounced for polarization parallel to the $\boldsymbol{b}$-axis, which is along the

direction of largest conductivity [19, 24]. The mechanism of field-induced lattice polarization can satisfactorily explain the anisotropy in the van der Waals plane of both $ReS_2$ and $ReSe_2$ crystals.

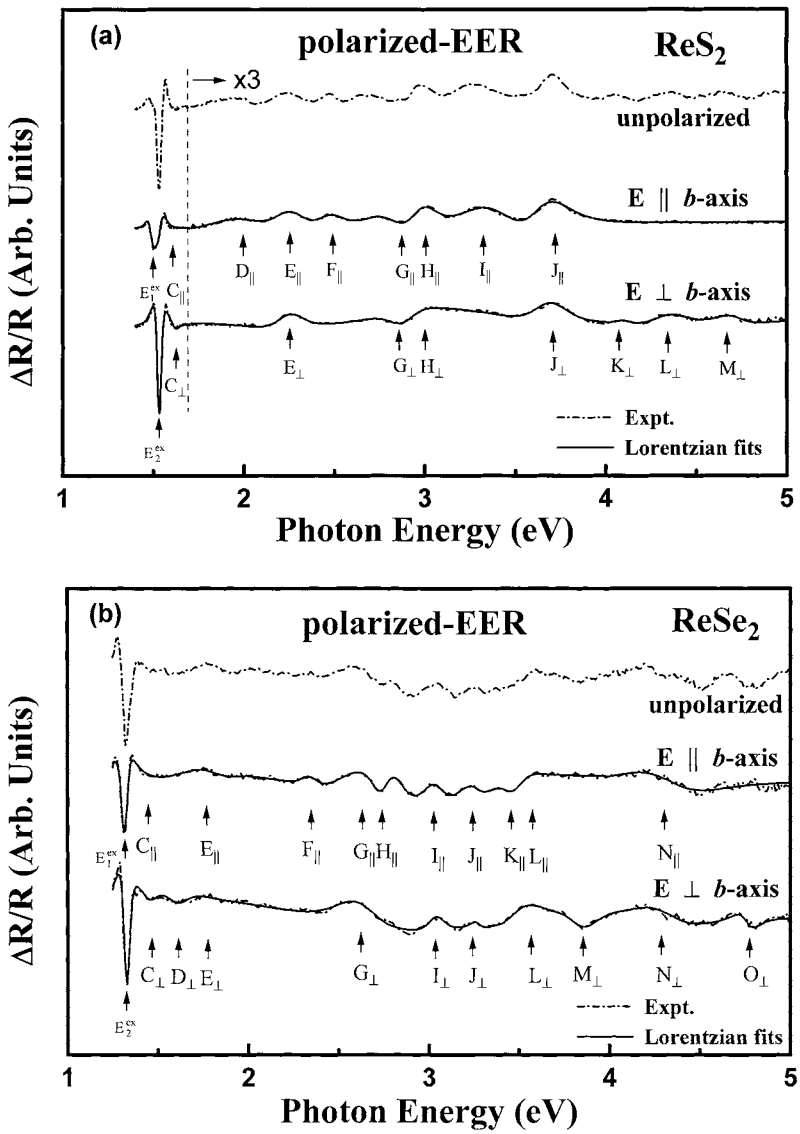


**Figure 2.** The polarized EER spectra of (a) $ReS_2$ and (b) $ReSe_2$ in the energy range of 1.3–5 eV. The dashed lines are experimental results derived from the EER measurements and the solid lines are least-squares fits to the Aspnes derivative line-shape functional form [13]. The transition energies (denoted as Roman letters) obtained from the line shape fits are indicated by arrows.

Based on the present experimental measurements and the existing theoretical calculation, the most prominent features of band-edge excitons ($E_1^{ex}$ and $E_2^{ex}$) can be correlated to the nonbonding Re 5d $t_{2g}$ ($d_{xy}$, $d_{x^2-y^2}$) to 5d$t_{2g}^*$ transitions. The features $C_\parallel$ and $C_\perp$ in figures 2(a) and 2(b) are assigned as the Re d to X p interband excitonic transitions. The reason for such an

**Table 2.** Energy positions of the excitonic and interband transitions observed in the polarized EER spectra of $ReSe_2$ together with the assignments of transition origins. The subscripts '$\|$' and '$\perp$' respectively refer to the $\boldsymbol{E} \parallel \boldsymbol{b}$ and $\boldsymbol{E} \perp \boldsymbol{b}$ polarizations.

| Feature | Energy position (eV) | The assignments of transition origins |
|---|---|---|
| $E_1^{ex}$ [a] | $1.309 \pm 0.005$ | Nonbonding Re 5d $t_{2g} \rightarrow$ nonbonding Re 5d $t_{2g}^*$ |
| $E_2^{ex}$ [a] | $1.326 \pm 0.005$ | Nonbonding Re 5d $t_{2g} \rightarrow$ nonbonding Re 5d $t_{2g}^*$ |
| $E_1^{ex}$ [b] | $1.315 \pm 0.005$ | Nonbonding Re 5d $t_{2g} \rightarrow$ nonbonding Re 5d $t_{2g}^*$ |
| $E_2^{ex}$ [b] | $1.330 \pm 0.005$ | Nonbonding Re 5d $t_{2g} \rightarrow$ nonbonding Re 5d $t_{2g}^*$ |
| $C_\|$ [b] | $1.450 \pm 0.005$ | Nonbonding Re 5d $t_{2g} \rightarrow$ Se 4p states |
| $C_\perp$ [b] | $1.461 \pm 0.005$ | Nonbonding Re 5d $t_{2g} \rightarrow$ Se 4p states |
| $D_\|$ [b] | not observed | |
| $D_\perp$ [b] | $1.61 \pm 0.01$ | Re 5d/Se 4p bonding $\rightarrow$ Re 5d/Se 4p antibonding |
| $E_\|$ or $E_\perp$ [b] | $1.76 \pm 0.01$ | Re 5d/Se 4p bonding $\rightarrow$ Re 5d/Se 4p antibonding |
| $F_\|$ [b] | $2.35 \pm 0.01$ | Re 5d/Se 4p bonding $\rightarrow$ Re 5d/Se 4p antibonding |
| $F_\perp$ [b] | not observed | |
| $G_\|$ or $G_\perp$ [b] | $2.64 \pm 0.01$ | Re 5d/Se 4p bonding $\rightarrow$ Re 5d/Se 4p antibonding |
| $H_\|$ [b] | $2.73 \pm 0.01$ | Re 5d/Se 4p bonding $\rightarrow$ Re 5d/Se 4p antibonding |
| $H_\perp$ [b] | not observed | |
| $I_\|$ or $I_\perp$ [b] | $3.03 \pm 0.01$ | Re 5d/Se 4p bonding $\rightarrow$ Re 5d/Se 4p antibonding |
| $J_\|$ or $J_\perp$ [b] | $3.24 \pm 0.01$ | Re 5d/Se 4p bonding $\rightarrow$ Re 5d/Se 4p antibonding |
| $K_\|$ [b] | $3.45 \pm 0.01$ | Re 5d/Se 4p bonding $\rightarrow$ Re 5d/Se 4p antibonding |
| $K_\perp$ [b] | not observed | |
| $L_\|$ or $L_\perp$ [b] | $3.58 \pm 0.01$ | Re 5d/Se 4p bonding $\rightarrow$ Re 5d/Se 4p antibonding |
| $M_\|$ [b] | not observed | |
| $M_\perp$ [b] | $3.85 \pm 0.01$ | Re 5d/Se 4p bonding $\rightarrow$ Re 5d/Se 4p antibonding |
| $N_\|$ or $N_\perp$ [b] | $4.30 \pm 0.01$ | Re 5d/Se 4p bonding $\rightarrow$ Re 5d/Se 4p antibonding |
| $O_\|$ [b] | not observed | |
| $O_\perp$ [b] | $4.78 \pm 0.01$ | Re 5d/Se 4p bonding $\rightarrow$ Re 5d/Se 4p antibonding |

[a] Derived from the room temperature results of [25].
[b] This work.

assignment is suggested by the low temperature PzR measurements of $ReS_2$ where a series of sharp features are observed at the same energy location [19]. From the EER spectra in figure 2, the structures at higher energies (i.e. features $D_\|$–$M_\perp$ for $ReS_2$ and $D_\perp$–$O_\perp$ for $ReSe_2$) are attributed to interband transitions from states of largely chalcogen X p character to (Re 5d $e_g^*$)–(X p) hybrid states. With the results of DOS calculations [17], polarized EER measurements and the optical absorption measurements [4], a probable band structure schemes consistent with the assignments in tables 1 and 2 for $ReX_2$ is constructed and is shown in figure 3. The band structure of $ReX_2$ is composed of three main bands separated by an energy gap. The lowest band consists of the chalcogen X s band; the next band is mainly X p hybridized with Re 5d. Three Re 5d orbitals form a non-bonding $t_{2g}$ band with $d_{z^2}$ at the bottom hybridized with X p and $d_{x^2-y^2}$ and $d_{xy}$ at the top of the band. The bottom of the conduction band is composed mainly of Re 5d states mixed with a small amount of X p orbitals. The antibonding Re 5d $t_{2g}^*$ band overlaps with the Re 5d $e_g^*$ band.

## 4. Summary

In summary, the polarization-dependent EER measurements of $ReS_2$ and $ReSe_2$ have been carried out. The $\boldsymbol{E} \parallel \boldsymbol{b}$ polarization spectra present distinct transition features from those of the $\boldsymbol{E} \perp \boldsymbol{b}$ polarization illustrating in-plane anisotropic properties of $ReX_2$. The mechanism of

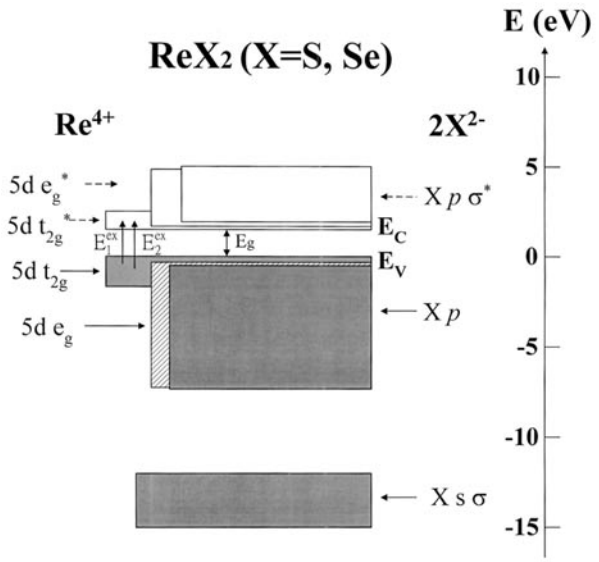


**Figure 3.** The energy band-structure scheme of $ReX_2$ (X = S, Se).

field lattice interaction is proposed to account for the in-plane anisotropy of the $ReX_2$ crystals. The structures of excitonic and interband transitions with optical polarizations along the ***b***-axis and perpendicular to the ***b***-axis are respectively examined and evaluated. Based on the results of polarized EER and previous optical absorption measurements with appropriate transition assignments, a probable energy band structure scheme for $ReX_2$ is proposed.

## Acknowledgments

The authors C H Ho and K K Tiong would like to acknowledge the support of the National Science Council of Republic of China under project No NSC89-2112-M-019-006 and P C Yen and Y S Huang acknowledge support under project No NSC89-2112-M-011-002.

## References

[1] Wilson J A and Yoffe A D 1969 *Adv. Phys.* **18** 193
[2] Wildervanck J C and Jellinek F 1971 *J. Less-Common Met.* **24** 73
[3] Ho C H, Liao P C, Huang Y S, Yang T R and Tiong K K 1997 *J. Appl. Phys.* **81** 6380
[4] Ho C H, Huang Y S, Tiong K K and Liao P C 1998 *Phys. Rev.* B **58** 16 130
[5] Broadbent H S, Slangh L H and Jarvis N L 1954 *J. Am. Chem. Soc.* **76** 1519
[6] Harris S and Chianelli R R 1984 *J. Catal.* **86** 400
[7] Koffyberg F P, Dwight K and Wold A 1979 *Solid State Commun.* **30** 433
[8] Wheeler B L, Leland J K and Bard A J 1986 *J. Electrochem. Soc.* **133** 358
[9] Friemelt K, Lux-Steiner M-Ch and Bucher E 1993 *J. Appl. Phys.* **74** 5266
[10] Parkinson B A, Ren J and Whangbo M-H 1991 *J. Am. Chem. Soc.* **113** 7833
[11] Cardona M, Shaklee K L and Pollak F H 1967 *Phys. Rev.* **154** 696
[12] Huang Y S and Chen Y F 1988 *Phys. Rev.* B **38** 7997
[13] Aspnes D E 1980 *Optical Properties of Semiconductors (Handbook on Semiconductors Vol 2)* ed M Balkanski (Amsterdam: North-Holland) p 109
[14] Kelty S P, Ruppert A F, Chianelli R R, Ren J and Whangbo M-H 1994 *J. Am. Chem. Soc.* **116** 7857
[15] Raybaud P, Hafner J, Kresse G and Troulhoat H 1997 *J. Phys.: Condens. Matter* **9** 11 107

[16] Ho C H, Liao P C, Huang Y S and Tiong K K 1997 *Phys. Rev.* B **55** 15 608
[17] Ho C H, Huang Y S, Chen J L, Dann T E and Tiong K K 1999 *Phys. Rev.* B **60** 15 766
[18] Ho C H, Huang Y S and Tiong K K 1999 *Solid State Commun.* **109** 19
[19] Ho C H, Huang Y S, Tiong K K and Liao P C 1999 *J. Phys.: Condens. Matter* **11** 5367
[20] Alcock N W and Kjekshus A 1965 *Acta Chem. Scand.* **19** 79
[21] Ho C H, Huang Y S, Liao P C and Tiong K K 1999 *J. Phys. Chem. Solids* **60** 1797
[22] Huang Y S, Chen H M, Chang C J and Jan G J 1985 *Chin. J. Phys.* **23** 144
[23] Weiser G 1973 *Surf. Sci.* **37** 175
[24] Tiong K K, Ho C H and Huang Y S 1999 *Solid State Commun.* **111** 635
[25] Huang Y S, Ho C H, Liao P C and Tiong K K 1997 *J. Alloys Compounds* **262/263** 92